Dramatic Pressure-Dependent Quenching Effects in Supercritical CO_2 Assessed by the Fluorescence of 4′-Dimethylamino-3-hydroxyflavone. Thermodynamic versus Kinetics Control of Excited-State Intramolecular Proton Transfer

Monica Barroso,[†] Nitin Chattopadhyay,[‡] Andrey S. Klymchenko,[§] Alexander P. Demchenko,[||] Luis G. Arnaut,*[,†] and Sebastião J. Formosinho[†]

Department of Chemistry, Coimbra University, P-3004-535 Portugal, Department of Chemistry, Jadavpur University, Calcutta 700 032, India, Faculté de Pharmacie, Laboratoire de Pharmacologie et Physicochimie, Université Louis Paster, BP 24, 67401 Illkirch, France, and The Palladin Institute of Biochemistry, Kiev 01030 Ukraine

Received: July 11, 2006; In Final Form: October 3, 2006

Steady-state fluorescence of 4′-dimethylamino-3-hydroxyflavone (DMA3HF) was observed in supercritical carbon dioxide ($scCO_2$). Excited-state intramolecular proton transfer (ESIPT) occurs resulting in two well-separated emission bands corresponding to the normal and tautomer forms. As the $scCO_2$ density exceeds 0.7 g/mL, the relative intensity of the two bands tends to a constant value, comparable to that observed for organic solvents with $E_T(30) = 33.0 \pm 0.5$ kcal/mol, such as toluene and di-*n*-butyl ether. At lower densities, the substantial decrease of the total fluorescence intensity (a 600-fold decrease as the pressure decreases from 100 to 80 bar) is accompanied by an even more accentuated decrease of the tautomer fluorescence. This can be explained by a shift in the equilibrium between normal and tautomer forms, concomitant with a more efficient quenching of the less solvated fluorophore, that may change the thermodynamic control of the relative population of the two emissive species to a kinetic control.

Introduction

Supercritical carbon dioxide ($scCO_2$) is known for its applications as an extracting solvent as well as a reaction environment.[1−3] Probably, the most interesting property of $scCO_2$ as a reaction solvent is the tunability of the medium properties, such as local density, by changing the pressure under isothermal conditions.[4−6] Fluorometric techniques find themselves the most effective methods for characterizing the properties of supercritical fluids, because of the high sensitivity of these techniques and the strong response of some fluorophores to solvent perturbations.

4′-Dialkylamino-3-hydroxyflavones undergo excited-state intramolecular proton transfer (ESIPT) in different environments, similar to the parent 3-hydroxyflavone (3HF),[7−12] giving rise to dual fluorescence. The higher energy band corresponds to the normal (N*) excited state, whereas the lower energy one corresponds to the tautomeric form (T*) that originates from the ESIPT reaction. The extension of the π-electronic system and the introduction of electron-donor substituents lead to an enhanced sensitivity of the positions of these bands (λ_{N^*}, λ_{T^*}) and, especially, their intensity ratios (I_{N^*}/I_{T^*}), to the properties of molecular environment. The strong influence that the microenvironment exerts on the spectroscopic parameters of this family of compounds motivated their widespread use as fluorescent probes for various purposes.[11,13−17]

The present work focuses on the fluorescence properties of 4′-dimethylamino-3-hydroxyflavone (DMA3HF), a remarkably sensitive fluorophore, as a function of the pressure and temperature of $scCO_2$. The evaluation of polarity and H-bonding in $scCO_2$ is facilitated by the large amount of experimental data available for DMA3HF and for the closely related 4′-diethylamino-3-hydroxyflavone (DEA3HF) fluorescent probe in different liquid solvents. The large dipole moment of the N* state in these species and, therefore, its strong solvent-dependent stabilization leads to reversible ESIPT reactions, at least in solvents without strong quenching effects, where fluorescence lifetimes are of the order of nanoseconds.[18,19] This makes the fluorescence of the normal and tautomer bands strongly dependent on the polarity and hydrogen-bonding properties of the environment, and explains the dramatic response of DMA3HF to changes in its solvation shell. We have also attempted to resolve the controversy on the polarity of the $scCO_2$ microenvironment in terms of the $E_T(30)$ parameter, using literature values of I_{N^*}/I_{T^*} for DMA3HF[18,19] and DEA3HF[14,20] in various homogeneous solvents of different polarities. The I_{N^*}/I_T ratio also provides insight into the thermodynamics and kinetics of ESIPT in $scCO_2$ in different pressure regimes.

Experimental Section

DMA3HF was synthesized as described elsewhere.[21,22] The purity of the compound was checked spectroscopically before use. Absorption and emission spectra were recorded using a Shimadzu UV-2001 spectrophotometer and a SPEX Fluorolog-3 spectrofluorimeter, respectively. The supercritical fluids setup has been described elsewhere.[23,24] For the absorption and emission studies, the samples were prepared by depositing a small amount of solid DMA3HF onto a sapphire window of the cell. The cell was then evacuated and filled with CO_2 after thermostating at the desired temperature. The concentrations of

* To whom correspondence should be addressed. E-mail: lgarnaut@ci.uc.pt.
[†] Coimbra University.
[‡] Jadavpur University.
[§] Université Louis Paster.
[||] The Palladin Institute of Biochemistry.

10.1021/jp0643606 CCC: $33.50
Published on Web 11/22/2006

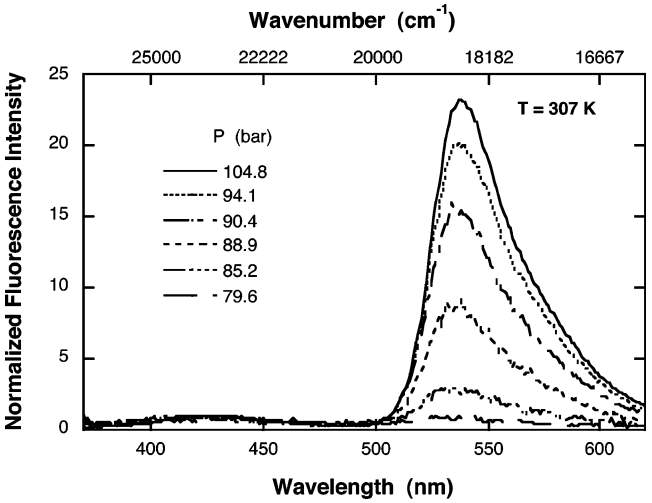

Figure 1. Fluorescence spectra of DMA3HF in $scCO_2$ at different pressures and $T = 307$ K. The spectra are normalized to the maximum of the normal band (428 nm) to emphasize the change in the relative intensities of the normal and tautomer bands. Excitation wavelength was 350 nm.

the samples were lower than 10^{-4} M, and covered a factor of 5 in concentrations. To control and measure the temperature in the cell, a thermostatic bath and a PT100 sensor were used (±0.1°). The pressure inside the cell was measured using an OMEGA DP20 digital pressure indicator (±0.25%).

Results

DMA3HF in $scCO_2$ gives rise to dual fluorescence when photoexcited to the S_1 state, as observed before in liquid solutions[18] and in phospholipid membranes for this dye[11] and its derivatives.[8,9,12−14,22] It is pertinent to point out here that, unlike in common fluid solvents, in $scCO_2$ this probe also gives rise to fluorescence from the S_2 state. This observation is very similar to our previous observation with the parent compound 3HF in $scCO_2$,[16,17] and with some other similar compounds in the vapor phase as shown previously by Nagaoka et al.[25] In the present article, we focus only on the S_1 emissions from the normal and the tautomeric species.

Figure 1 shows the fluorescence intensities of the normal (I_{N^*}) and the tautomer (I_{T^*}) of DMA3HF in $scCO_2$, as a function of pressure under isothermal conditions. The fluorescence spectra, normalized at the normal emission maximum, clearly indicate a decrease in the tautomer band intensity with a decrease in the pressure on the system. The position of the first maximum of the absorption band ($\lambda_{max} = 375$ nm, $\bar{\nu} = 26\,667$ cm $^{-1}$) is virtually independent of the pressure, and those of the normal and taumomer emission bands undergo small blue shifts with a decrease in pressure. As the pressure increases from 80 to 100 bar at 307 K, the normal emission band shifts from $\bar{\nu}_{N^*} = 23\,670$ to 23 420 cm^{-1}, and the tautomer band shifts from $\bar{\nu}_{T^*} = 18\,690$ to 18 590 cm^{-1}. These red shifts indicate a better solvation of the probe and the stabilization of the N* and T* states on an increase of pressure.

Remarkably, the red shift of the tautomer band with an increase in pressure is accompanied by a dramatic increase in its fluorescence intensity by a factor of 600 in this pressure range, whereas that of the normal band increases by a factor of 30 only. Since this effect is independent of probe concentration in the $(2 - 10) \times 10^{-5}$ M range, it is unlikely that it is related to aggregation.

Because of the wide separation of the emission bands corresponding to the two forms, there is practically no overlap between the two emissions. This allows one to calculate I_{N^*}/I_{T^*} directly from the absolute heights of the corresponding maxima. The variation of I_{N^*}/I_{T^*} shows characteristic pressure dependences at each temperature (Figure 3). In the temperature range studied in this work, the intensity ratio rapidly decreases as the pressure is increased until a certain pressure is attained (P_{min}). There are associated bathochromic shifts of 250 and 100 cm^{-1} in the normal and tautomer emissions, respectively, with this increase in pressure.

A further increase in the pressure does not affect I_{N^*}/I_{T^*}. The value of I_{N^*}/I_{T^*} at P_{min} is the lowest value that this ratio can attain at a given temperature, and in the range of temperatures studied, it is very weakly temperature dependent. With an increase in temperature, P_{min} shifts toward higher pressure and the sharpness of the break point is reduced. Thus, the effect of temperature on the I_{N^*}/I_{T^*} ratio is strong at low pressures but tends to disappear at high pressures. This behavior has a remarkable similarity with the results for 3HF and benzil,[16,23] which further contributes to exclude probe aggregation as the reason for the changes observed in the I_{N^*}/I_{T^*} ratio.

Discussion

Many of the parameters employed to characterize the solvation properties of $scCO_2$, such as the bulk relative permittivity (ϵ_r), the refractive index (n) or the pyrene I_1/I_3 scale, are related to the density (ρ) of $scCO_2$. For example using the dependence of ϵ_r and n on ρ[26] and its value at 307 K, ϵ_r increases from 1.316 at 80 bar to 1.435 at 100 bar and 1.583 at 300 bar, whereas n increases from 1.125 to 1.168 and to 1.217, in the same pressure range. We observed a similar increase in the I_1/I_3 scale, from 0.87 at 80 bar to ca. 1.0 at 100 bar at 308 K,[27] in agreement with the literature values.[26] When the electronic polarizability $f(n) = (n^2 - 1)/(2n^2 + 1)$ is employed to characterize $scCO_2$, the values obtained are lower than 0.1 at pressures below 100 bar; that is, its electronic polarizability is half of that typical of organic solvents. The polarity function $f(\epsilon_r) = (\epsilon_r - 1)/(2\epsilon_r + 1)$ also gives very low values, $f(\epsilon_r) < 0.113$ at pressures below 100 bar, even when compared with apolar solvents such as hexane, for which $f(\epsilon_r) = 0.185$.[14] The pyrene I_1/I_3 scale suggests a somewhat larger polarity, similar to that of toluene when the temperature is 308 K and the pressure is higher than 100 bar. All of these data suggest that $scCO_2$ has a low electronic polarizability and a low polarity. Yet, it is renowned for being a remarkably good solvent. Apparently, these polarity scales do not reflect all of the solvation properties of $scCO_2$.

Another very popular scale to assess the polarity of a solvent is the $E_T(30)$ empirical scale.[9,28] However, the betaine dye employed in this scale is insoluble in $scCO_2$ and indirect measurements of $E_T(30)$, using correlations with measurable properties, have led to conflicting results. Hyatt used a secondary standard to obtain $E_T(30) = 33.8$ kcal/mol for both liquid and $scCO_2$.[29] Ikushima and co-workers used several empirical correlations to conclude that $E_T(30)$ increases from 31.1 to 31.8 kcal/mol with an increase in density.[30] We approached this issue using the correlation between $\log(I_{N^*}/I_{T^*})$ of DMA3HF or DEA3HF and $E_T(30)$ observed for different solvents. Figure 3 shows the plot of $\log(I_{N^*}/I_{T^*})$ as a function of $E_T(30)$ using the data available in the literature.[14,18,19] Introducing the extreme $\log(I_{N^*}/I_{T^*})$ values measured in $scCO_2$ in this plot gives the range of $E_T(30)$ values that characterize $scCO_2$ at different pressures and temperatures. As discussed above, the value of I_{N^*}/I_{T^*} at P_{min} is the lowest value that this ratio can attain. It corresponds to $E_T(30) = 33.0 \pm 0.5$ kcal/mol, in very good agreement with the value reported by Hyatt and supporting the view that solvent

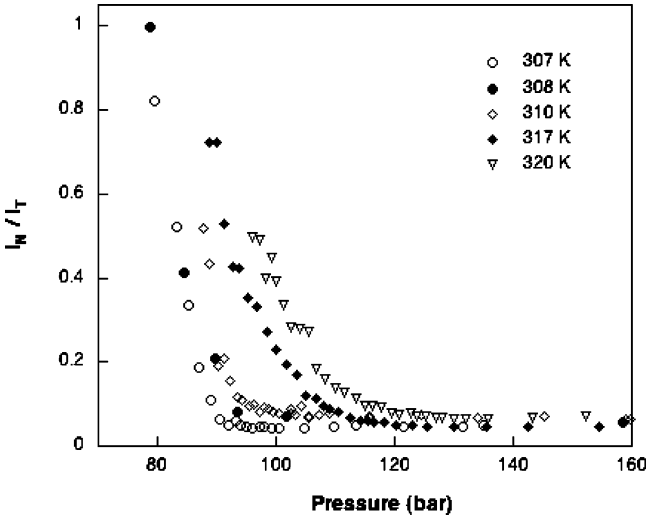

Figure 2. Plot of I_{N*}/I_{T*} of DMA3HF in $scCO_2$ as a function of pressure at different temperatures. The temperatures are given in the inset.

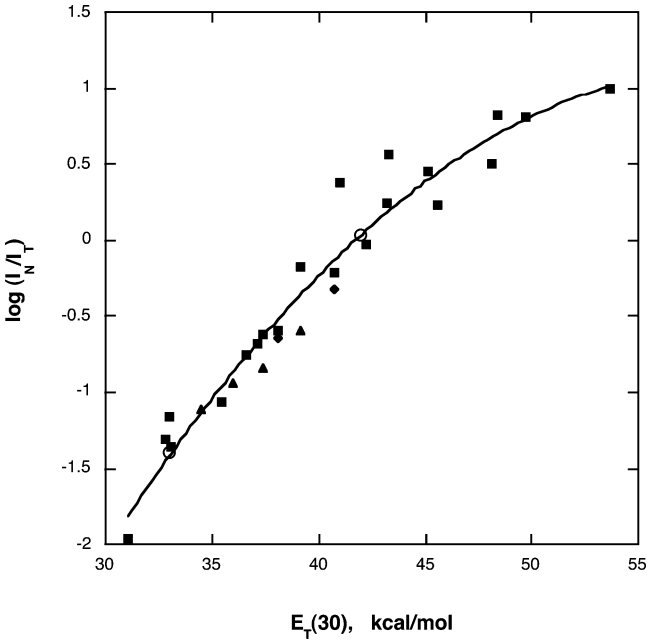

Figure 3. Plot of logarithm of I_{N*}/I_{T*} of DMA3HF (diamonds[18] and triangles[19]) and DEA3HF (squares)[14] as a function of solvent polarity function $E_T(30)$[31] and of the band separation $\bar{\nu}_N - \bar{\nu}_T$ in different solvents. The circles are the interpolations of the limiting ratios obtained with DMA3HF in $scCO_2$.

properties of $scCO_2$ resembles those of toluene ($E_T(30) = 33.9$[31]). Moreover, the observed separation between normal and tautomer fluorescence bands $\bar{\nu}_N - \bar{\nu}_T$ (4940 cm^{-1}) and the I_{N*}/I_{T*} ratio (0.04) correspond well to the general solvent polarity dependence (Figure 4). This indicates that $scCO_2$ is comparable to organic solvents at pressures higher than 100 bar and that at least for such pressures the ESIPT equilibrium for the dye is reached on the early steps of emission. Thus, our methodology of polarity measurements based on the I_{N*}/I_{T*} ratio is justified for $scCO_2$ at high pressures.

The normal and tautomer fluorescence bands are blue-shifted with respect to their energies in organic solvents, but the position of the absorption band in $scCO_2$ is in reasonable agreement with the position expected for a solvent with its low polarizability function $f(n)$, $\bar{\nu} = 26\,667$ vs $27\,128$ cm^{-1} at 100 bar and 307 K. The same is also true for the position of the normal fluorescence band, given the polarity function $f(\epsilon_r)$ of $scCO_2$.

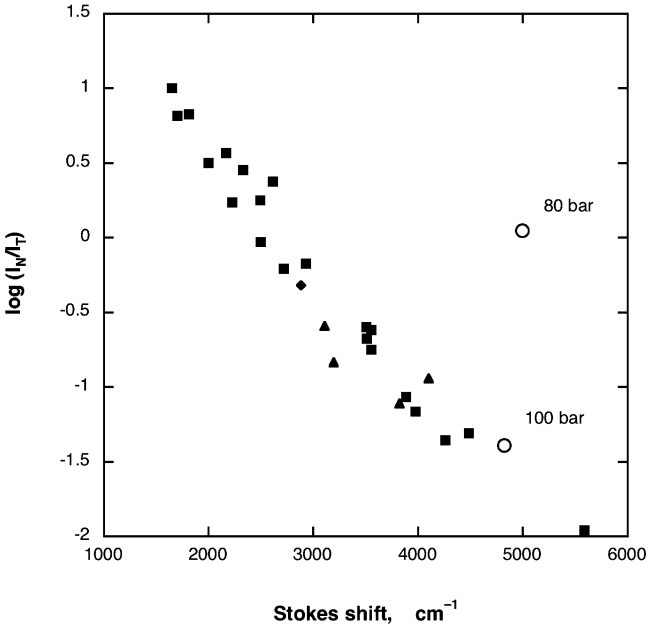

Figure 4. Correlation between $\log(I_{N*}/I_{T*})$ and band separations $\bar{\nu}_N - \bar{\nu}_T$ in different solvents. Symbols and references as in the previous figure.

The position of the tautomer fluorescence band is only slightly less blue-shifted than expected from the $f(\epsilon_r)$ of $scCO_2$ (17 930 vs 18 590 cm^{-1} at 100 bar and 307 K). The consequence of such blue shifts is that measurements of $scCO_2$ polarity based on the absolute positions of absorption or fluorescence bands tend to underestimate its solvent properties. This explains the discrepancies between earlier measurements of the $E_T(30)$ of $scCO_2$. On the other hand, measurements of the Stokes shifts give a better picture of the solvent properties of $scCO_2$. This is apparent in the work of Reynolds et al.,[32] which observed Stokes shifts of Coumarin 153 in $scCO_2$ that are intermediate between those observed in diisopropyl ether and diethyl ether. The Stokes shift observed for DMA3HF in $scCO_2$, 3247 cm^{-1} at 100 bar and 2997 cm^{-1} at 80 bar, is also similar to that of DEA3HF in di-*n*-butyl ether.

Unexpectedly, there is dramatic increase in I_{N*}/I_{T*} with a decrease in pressure that leads to an apparent increase in $E_T(30)$ at lower pressures. The largest I_{N*}/I_{T*} ratio measured in this work was 1.1, at 80 bar and 307 K. According to Figure 3, it should correspond to $E_T(30) = 42$ kcal/mol (i.e., larger than that of acetone). The remarkable variation of I_{N*}/I_{T*} with pressure contrasts with the insensitivity of the energies of absorption and emission bands with pressure. For example, the decrease in pressure from 100 to 80 bar at 307 K leads to a blue shift of the emission bands that is coupled with an increase in I_{N*}/I_{T*} from 0.04 to 1.1. In organic solvents, a decrease in solvent polarity also leads to a blue shift of the emission bands but decreases the I_{N*}/I_{T*} ratio.[28] Analysis of $\log(I_{N*}/I_{T*})$ vs band separation $\bar{\nu}_N - \bar{\nu}_N$ for the low pressure (80 bar) reveals a strong deviation of the data point upward from the correlation observed for organic solvents (Figure 4). This indicates that the dye does not behave like in organic solvent when the density of $scCO_2$ is low namely the extent of ESIPT is less than expected from the relative band position. The unexpected increase of I_{N*}/I_{T*} at lower pressures, where the polarity of $scCO_2$ should be lower, cannot be assigned to H-bonding of CO_2 molecules with the dye, because at lower densities this interaction should be even lower (thus contributing to the opposite, decrease in I_{N*}/I_{T*}). Additionally, it cannot be H-bonding between DMA3HF molecules, because the I_{N*}/I_{T*} ratio is independent of the

concentration of DMA3HF. These data show that changes in the PT barrier, namely due to intermolecular hydrogen bonding, are not responsible for the decrease of the tautomer fluorescence at low pressures.

The explanation for increase of the I_{N*}/I_{T*} ratio at low CO_2 pressures must also accommodate the fluorescence dynamics of 4′-dialkylamino-3-hydroxyflavones in organic solvents. It was recently shown that their excited states have nanosecond lifetimes and undergo reversible ESIPT,[18,19] as the fluorescence decay rates are much slower than the ESIPT rates. Under reversible conditions, the I_{N*}/I_{T*} ratio is governed by the ESIPT equilibrium. However, if the rates of nonradiative deactivation become comparable to the ESIPT rates, the I_{N*}/I_{T*} ratio will be controlled by the forward ESIPT rate as well as by the rates of deactivation of the two states. This changes the I_{N*}/I_{T*} ratio from a thermodynamic to kinetic control.

The strong increase in the I_{N*}/I_{T*} ratio when the pressure is lowered, the associated decrease in fluorescence intensity, and the fact that these effects are more pronounced at higher temperatures show that, at low pressures, the normal form can explore more efficiently the nonradiative decay channels to the ground state. It is now widely recognized that conical intersections are a significant part of such channels. For example, Robb and co-workers found an extended seam of conical intersection with a sloped topology lying parallel to the ESIPT path of *o*-hydroxyphenyl triazines,[33] which can be accessed at any point along the reaction path. The presence of conical intersections in the vicinity of the Franck-Condon (FC) state formed upon excitation of the normal form, explains the sensitivity of DMA3HF fluorescence to the CO_2 pressure. The pressure dependence of the fluorescence and of the I_{N*}/I_{T*} ratio can be explained by at least three mechanisms.

Mechanism I: At low pressures, we have a gas-like medium with a slow vibrational relaxation from the FC state, and a significant fraction of the "hot" DMA3HF molecules finds its way to the conical intersection before their thermalization to the relaxed (fluorescent) state.

Mechanism II: The normal form is nevertheless thermalized efficiently, but the poorly solvated DMA3HF molecules at low CO_2 densities have an increased conformational flexibility and may reach the conical intersection more efficiently.

Mechanism III: The normal form is still thermalized efficiently, but the incomplete solvation of DMA3HF molecules close to the critical point of CO_2 exposes them to collisions with rapidly moving individual CO_2 molecules, because $scCO_2$ is a micro-heterogeneous system with isolated molecules and clusters, and the transfer of momentum in the collisions takes the system to the conical intersection.

The increase of the radiationless decays in the first mechanism takes place before the fluorescent state is reached and does not require a decrease in the fluorescence lifetime. On the other hand, mechanisms II and III involve a more efficient quenching of the fluorescent state at low CO_2 pressures by either an intramolecular or an intermolecular process, respectively. It is tempting to associate the degree of conformational flexibility invoked by the second mechanism with the strength of viscosity-type solute−solvent interactions.[34] However, viscosity is strongly correlated with density, and the treatment of our data as a function of the viscosity does not provide any new insight. On the other hand, the increased conformational flexibility should lead to the increase of the bandwidths at half-height, $\Delta\bar{\nu}_{1/2}$. Careful examination of the pressure dependence of $\Delta\bar{\nu}_{1/2}$ at $T = 307$ K reveled nearly constant $\Delta\bar{\nu}_{1/2}$ values. For the tautomer emission, which is amenable to more precise measurements, we obtained $\Delta\bar{\nu}_{1/2} \approx 1425 \pm 10$ cm^{-1} from 100 to 83 bar. Thus, conformation flexibility changes can be excluded as the cause for the observed dependence of the I_{N*}/I_{T*} ratio on pressure. The collisional quenching of the last mechanism is of ballistic, rather than chemical, nature. It depends on the competition between the frequency of the collisions and the ESIPT rate. The simple kinetic theory of gases gives the indication that the collision frequency of CO_2 molecules at 307 K and 80 bar is 5×10^{11} s^{-1}. The final assessment of mechanisms I and III requires ultrafast lifetime measurements in $scCO_2$ and detailed kinetic analysis of the reversibility of the processes involved. We are presently developing and installing the technology required for such measurements, but meanwhile a theoretical analysis of the ESIPT rates can provide more insight into our system.

TABLE 1: Bond Lengths, Bond Dissociation Energies, Vibrational Frequencies of Phenol, and Ionization Potentials and Electron Affinities of Phenoxy Radical, Employed in the Calculation of ESIP[a]

	l_{AH},eq/Å	D^0_{298}/kcal/mol	$\bar{\nu}_{AH}$/cm^{-1}	I_P/eV	E_A/eV
RO−H	0.956	86.5	3650	8.56[b]	2.253

[a] Data from ref 39 and http://www.webbook.nist.gov. [b] For the singlet-state reactions, the singlet state energy (3.10 eV) was subtracted from I_P.

The explanation presented above may not be sufficient, since in addition to quenching there is a re-distribution of the band intensities. They indicate changes of state energetics that should influence ESIPT rate, and these changes have to be taken into account.

According to the recent formulation of the intersecting/interacting-state model (ISM) for atom and proton-transfer reactions,[35−37] the reaction coordinate of a proton-transfer reaction, AH + $^-$B → A$^-$ + HB, is a linear interpolation between the Morse curves of HA and HB along the reaction coordinate

$$V_{cl}(n) = (1 - n)V_{HA} + nV_{HB} + n\Delta V^0 \qquad (1)$$

where ΔV^0 is the classical reaction energy and the reaction coordinate n ($=n_{BC}$) is the bond order of the new bond formed in the course of the reaction. The Morse curves representing reactants and products are modified to account for electron inflow at the transition state

$$V_{HA} = D_{eHA}\left\{1 - \exp\left[-\frac{\beta_{HA}(l_{HA} - l_{HA,eq})}{m}\right]\right\}^2$$
$$V_{HB} = D_{eHB}\left\{1 - \exp\left[-\frac{\beta_{HB}(l_{HB} - l_{HB,eq})}{m}\right]\right\}^2 \qquad (2)$$

where the electrophilicity parameter m was defined by Parr[38]

$$m = \frac{I_P - E_A}{I_P + E_A} \qquad (3)$$

in terms of the ionization potential (I_P) and electron affinity (E_A) of the radicals corresponding to the HA and HB molecules. The data needed to represent the O−H bonds by Morse curves were taken from phenol and phenoxy radical and are shown in Table 1.

For DMA3HF in weakly polar organic solvents, the separation between N* and T* states on an energy scale is close to −1 kcal/mol,[18,19] and ΔV^0 in $scCO_2$ at 100 bar and 307 K is expected to be very close to this value, because the zero-point energy corrections of reactants and products are virtually

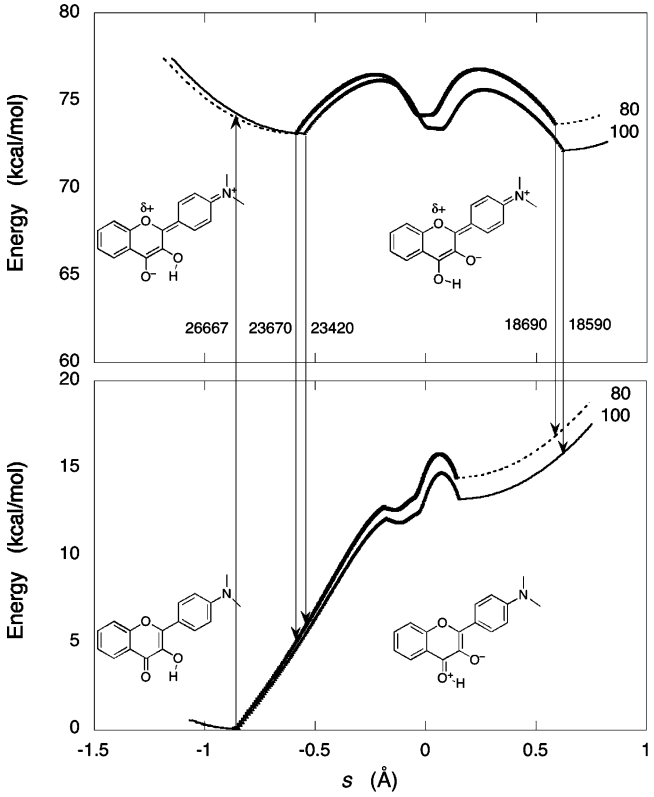

Figure 5. Relative energies of the states involved in ground and ESIPT of DMA3HF in $scCO_2$ at 100 and 80 bar. The thicker lines are the vibrationally adiabatic energies of the ISM reaction coordinate, and the thinner lines are harmonic curves extending that reaction coordinate to the Franck−Condon states. The reaction coordinate is defined as $s = \pm[(l_{AH} - l^{\ddagger}_{AH})^2 + (l_{BH} - l^{\ddagger}_{BH})^2]^{1/2}$. The energies are relative to the ground-state of the hydrogen-bonded normal form. The excited-state tautomer is stabilized by an increase in pressure but its fluorescence emission changes only by 0.3 kcal/mol because a similar stabilization takes place in the ground-state tautomer.

identical. The presence of a hydrogen bond in the reaction coordinate is taken into account using the Lippincott−Schroeder potential that relates A···B hydrogen bond distances (l_{AB}) to H-bond strengths (D_{0AB}), frequencies ($\bar{\nu}_{AB}$) and A···H ($l_{A\cdots H}$) or H···B ($l_{B\cdots H}$) bond lengths.[40] These bond lengths are then related to the respective bond orders, and the ISM reaction coordinate is calculated from the H-bonded reactants to the H-bonded products.

Figure 5 presents ISM calculations using the data in Table 1, $\Delta V^0 = -1$ kcal/mol at 100 bar and $+0.5$ kcal/mol at 80 bar, and $D_{0AB} = 1$ kcal/mol for the normal ground state. This H-bond energy is the value that reproduces the experimental $l_{AB} = 2.66$ Å of the normal form in ground state.[41,42] The other structures must have larger D_{0AB} values because of the presence of charges,[36] and we employed $D_{0AB} = 2$ kcal/mol for the normal and tautomer in the excited state, and $D_{0AB} = 5$ kcal/mol for the tautomer in the ground state.

Figure 5 presents vibrationally adiabatic potential curves, rather than classical potential curves, because zero-point energy corrections were added along the reaction coordinates.[35−37] The most significant effect of the zero-point energy corrections is the involvement of a potential well in the reaction coordinate, due to the loss of vibrational energy close to the transitions state. Finally, this figure also includes harmonic potential energy curves outside the range of the ISM reaction coordinate. These curves reflect the energy changes associated with the Franck−Condon transitions that lie along a distinct reaction coordinate, probably associated with the ring-breathing mode.[43]

Rather than focusing on the details of the calculations that do not change the overall picture of Figure 5, it is important to emphasize that all of the energy relations observed in this work are quasiquantitatively rationalized by the ISM reaction coordinate and by the subsidiary energy cycle. In particular, the increase in the energy of the excited-state tautomer with a decrease in pressure does not lead to a blue shift of the tautomer band because of the concomitant energy increase of the ground state tautomer. This is anticipated from the more unfavorable charge distribution of the tautomer in the ground state. Thus, the dramatic change in the I_{N^*}/I_{T^*} ratio can be explained by a 1.5 kcal/mol increase in the energy of the tautomer with respect to that of the normal form.

The kinetics of this system can also be rationalized by the ISM reaction coordinate that determines the interplay of forward and reverse ESIPT rates. In fact, ISM was designed to provide simple, yet accurate, estimates of reaction rates. Neglecting tunneling corrections, ISM expresses the rate constant for intramolecular proton transfers as[35−37]

$$k_{ISM} = c\bar{\nu}_{AB} \exp\left(-\frac{\Delta V^{\ddagger}_{ad}}{RT}\right) \qquad (4)$$

where $\Delta V^{\ddagger}_{ad}$ is, for each reaction path shown in Figure 5, the energy difference between its maximum and the energy of the H-bonded reactants. The rate constant calculated at 100 bar and 307 K ($\Delta V^0 = -1.0$ kcal/mol, $\bar{\nu}_{AB} = 59$ cm^{-1}, $\Delta V_{ad}{}^{\ddagger} = 3.0$ kcal/mol) is $k_{ISM} = 1.3 \times 10^{10}$ s^{-1}. In weakly polar solvents at room temperature, the experimental rate is 2×10^{10} s^{-1}.[18,19] This is in excellent agreement, further supporting the energy relations of Figure 5. At 80 bar ($\Delta V^0 = +0.5$ kcal/mol, $\bar{\nu}_{AB} = 59$ cm^{-1}, $\Delta V_{ad}{}^{\ddagger} = 3.6$ kcal/mol), the calculations give $k_{ISM} = 4.8 \times 10^9$ s^{-1}. Thus, the ESIPT rate constant should decrease by a factor of 3 when the pressure is decreased from 100 to 80 bar and contribute to the increase observed in the I_{N^*}/I_{T^*} ratio.

The ESIPT rate is only 1 order of magnitude smaller than the expected collision frequency with CO_2 molecules, and the ballistic quenching of mechanism III cannot be excluded on these grounds. On the other hand, the observation of emission from the S_2 state shows that other photophysical processes effectively compete with internal conversion and vibrational relaxation at low pressures, and mechanism I may also be relevant. The remarkable variety of processes occurring in DMA3HF at low CO_2 pressures and the information that they may provide on the environment of this probe will certainly stimulate further research in this area.

Conclusion

The present work shows that 3-hydroxyflavone analogues are useful probes to monitor the microheterogeneity of $scCO_2$ due to their high sensitivity to solvent perturbations. The polarity of the $scCO_2$ environment cannot be assessed exclusively by the absolute position of absorption or emission bands of probe molecules. In terms of the $E_T(30)$ scale, the minimum value that describes the $scCO_2$ polarity is 33.0 ± 0.5 kcal/mol and should only be employed for densities higher than 0.7 g/mL, which correspond, for example, to a pressure of 95 bar at 307 K. At low pressures, the dye loses part of its solvation shell. This may slow down the vibrational relaxation from the FC state to the fluorescent state and facilitate the radiationless decay of the vibrationally hot molecules directly to the ground state. The poor solvation of the dye may also expose it to collisional quenching also facilitating its radiationless decay. Thus, an incomplete solvation shell explains the paradox of a dramatic

decrease in fluorescence intensity with a decrease in pressure. Finally, our results also show that the thermodynamic control of the normal and tautomer relative emission intensities may be changed into a kinetic control by fine-tuning of the external pressure.

Acknowledgment. Financial supports from Fundação para a Ciência e a Tecnologia (Grant BD/1332/2000) and FEDER (Project POCTI/47267/QUI/2002) are gratefully acknowledged. We also acknowledge with thanks the financial support from GRICES, Government of Portugal, and DST, Government of India, through an Indo−Portuguese project.

References and Notes

(1) Baiker, A. *Chem. Rev.* **1999**, *99*, 453.
(2) Clifford, T. *Fundamentals of Supercritical Fluids*; Oxford University Press: London, 1999.
(3) Kendall, J. L.; Canelas, D. A.; Young, J. L.; DeSimone, J. M. *Chem. Rev.* **1999**, *99*, 543.
(4) Shing, K. S.; Chung, S. T. *J. Phys. Chem.* **1987**, *91*, 1674.
(5) Eckert, C. A.; Ziger, D. H.; Johnston, K. P.; Kim, S. *J. Phys. Chem.* **1986**, *90*, 2738.
(6) Debenedetti, P. G.; Mohamed, R. S. *J. Chem. Phys.* **1989**, *90*, 4528.
(7) McMorrow, D.; Kasha, M. *J. Phys. Chem.* **1984**, *88*, 2235.
(8) Swinney, T. C.; Kelley, D. F. *J. Phys. Chem.* **1991**, *95*, 10369.
(9) Chou, P.-T.; Martinez, M. L.; Clements, J. H. *J. Phys. Chem.* **1993**, *97*, 2618.
(10) Formosinho, S. J.; Arnaut, L. G. *J. Photochem. Photobiol. A: Chem.* **1993**, *75*, 21.
(11) Duportail, G.; Klymchenko, A. S.; Mely, Y.; Demchenko, A. *FEBS Lett.* **2001**, *508*, 196.
(12) Klymchenko, A. S.; Ozturk, T.; Pivovarenko, V. G.; Demchenko, A. *Tetrahedron Lett.* **2001**, *42*, 7967.
(13) Klymchenko, A. S.; Pivovarenko, V. G.; Ozturk, T.; Demchenko, A. *New J. Chem.* **2003**, *27*, 1336.
(14) Klymchenko, A. S.; Demchenko, A. *Phys. Chem. Chem. Phys.* **2003**, *5*, 461.
(15) Klymchenko, A. S.; Demchenko, A. *J. Am. Chem. Soc.* **2002**, *124*, 12372.
(16) Chattopadhyay, N.; Barroso, M.; Serpa, C.; Silva, M. I.; Arnaut, L. G.; Formosinho, S. J. *Chem. Phys. Lett.* **2004**, *387*, 263.
(17) Chattopadhyay, N.; Barroso, M.; Serpa, C.; Arnaut, L. G.; Formosinho, S. J. *Chem. Phys. Lett.* **2004**, *387*, 258.
(18) Shynkar, V. V.; Mely, Y.; Duportail, G.; Piémont, E.; Klymchenko, A. S.; Demchenko, A. *J. Phys. Chem. A* **2003**, *107*, 9522.
(19) Roshal, A. D.; Organero, J. A.; Douhal, A. *Chem. Phys. Lett.* **2003**, *379*, 53.
(20) Klymchenko, A. S.; Mely, Y. *Tetrahedron Lett.* **2004**, *45*, 8391.
(21) Ormson, M. S.; Brown, R. G.; Vollmer, F.; Rettig, W. *J. Photochem. Photobiol.* **1994**, *81*, 65.
(22) Klymchenko, A. S.; Duportail, G.; Ozturk, T.; Pivovarenko, V. G.; Mely, Y.; Demchenko, A. *Chem. Biol.* **2002**, *9*, 1199.
(23) Chattopadhyay, N.; Serpa, C.; Silva, M. I.; Arnaut, L. G.; Formosinho, S. J. *Chem. Phys. Lett.* **2001**, *347*, 361.
(24) Nunes, R. M. D.; Arnaut, L. G.; Solntsev, K. M.; Tolbert, L. M.; Formosinho, S. J. *J. Am. Chem. Soc.* **2005**, *127*, 11890.
(25) Nagaoka, S.-i.; Nagashima, U. *Chem. Phys.* **1989**, *136*, 153.
(26) Sun, Y.-P.; Bunker, C. E.; Hamilton, N. B. *Chem. Phys. Lett.* **1993**, *210*, 111.
(27) Serpa, C. Reacções Fotoinduzidas de Transferência de Electrão em Fluidos Supercríticos; University of Coimbra: Coimbra, Portugal, 2004.
(28) Ercelen, S.; Klymchenko, A. S.; Demchenko, A. *Anal. Chim. Acta* **2002**, *464*, 273.
(29) Hyatt, J. A. *J. Org. Chem.* **1984**, *49*, 5097.
(30) Ikushima, Y.; Saito, N.; Arai, M.; Arai, K. *Bull. Chem. Soc. Jpn.* **1991**, *64*, 2224.
(31) Reichardt, C. *Chem. Rev.* **1994**, *94*, 2319.
(32) Reynolds, L.; Gardecki, J. A.; Frankland, S. J. V.; Horng, M. L.; Maroncelli, M. *J. Phys. Chem.* **1996**, *100*, 10337.
(33) Paterson, M. J.; Robb, M. A.; Blancafort, L.; DeBellis, A. D. *J. Phys. Chem. A* **2005**, *109*, 7527.
(34) Troe, J. *Pure Appl. Chem.* **1997**, *69*, 841.
(35) Arnaut, L. G.; Pais, A. A. C. C.; Formosinho, S. J.; Barroso, M. *J. Am. Chem. Soc.* **2003**, *125*, 5236.
(36) Barroso, M.; Arnaut, L. G.; Formosinho, S. J. *ChemPhysChem* **2005**, *6*, 363.
(37) Arnaut, L. G.; Formosinho, S. J.; Barroso, M. *J. Mol. Struct.* **2005**, *786*, 207.
(38) Parr, R. G.; Szentpály, L. v.; Liu, S. *J. Am. Chem. Soc.* **1999**, *121*, 1922.
(39) *Handbook of Chemistry and Physics*, 3rd electronic ed.; CRC Press Inc.: Boca Raton, FL, 2001.
(40) Lippincott, E. R.; Schroeder, R. *J. Chem. Phys.* **1955**, *23*, 1099.
(41) Etter, M. C.; Urbanczyk-Lipkowska, Z.; Baer, S.; Barbara, P. F. *J. Mol. Struct.* **1986**, *144*, 155.167.
(42) Cornard, J. P.; Vrielynck, L.; Merlin, J. C.; Wallet, J. C. *Spectrochim. Acta* **1995**, *51A*, 913.
(43) Serpa, C.; Arnaut, L. G.; Formosinho, S. J.; Naqvi, K. R. *Photochem. Photobiol. Sci.* **2003**, *2*, 616.